J. Fluid Mech. (1996), vol. 320, pp. 395–416

Simple shear flow of suspensions of liquid drops

By XIAOFAN LI, R. CHARLES AND C. POZRIKIDIS

Department of Applied Mechanics and Engineering Sciences,
University of California at San Diego, La Jolla, CA 92093-0411, USA

(Received 5 August 1995 and in revised form 10 April 1996)

The shearing motion of monodisperse suspensions of two-dimensional deformable liquid drops with uniform interfacial tension is studied by means of numerical simulations. In the theoretical model, the drops are distributed randomly within a square that is repeated periodically in two directions yielding a doubly periodic flow. Under the assumption that inertial effects are negligible and the viscosity of the drops is equal to that of the suspending fluid, the motion is investigated as a function of the area fraction of the suspended drops and of the capillary number. The evolution of the suspension from an initial configuration with randomly distributed circular drops is computed using an improved implementation of the method of interfacial dynamics which is based on the standard boundary integral formulation for Stokes flow. The numerical procedure incorporates the method of multipole expansions to account for far-drop interactions, and interpolation through tables for computing the doubly periodic Green's function; the latter allows considerable savings in the cost of the computations. Dynamic simulations are carried out for suspensions with up to 49 drops within each periodic cell, for an extended period of time up to $kt = 60$, where k is the shear rate. Comparisons with previous numerical results for solid particles reveal that particle deformability and interfacial mobility play an important role in the character of the motion. The effects of particle area fraction and capillary number on the effective rheological properties of the suspension are discussed, and the statistics of the drop motion is analysed with reference to the drop-centre pair distribution function and probability density functions of drop aspect ratio and inclination. It is found that the effective rheological properties may be predicted with remarkable accuracy from a knowledge of the instantaneous mean drop deformation and orientation alone, even at high area fractions. Cluster formation is not as important as in suspension of solid particles. The apparent random motion of the individual drops, when viewed at a sequence of time intervals that are large compared to the inverse shear rate, is described in terms of an effective non-isotropic long-time diffusivity tensor, and the transverse component of this tensor is computed from the results of the simulations with some uncertainty.

1. Introduction

Deformable particles, such as gas bubbles, liquid drops, organic agglomerates, and biological cells, are the building blocks of a broad class of industrial and physiological fluids. Examples include bubbly liquids, fluid mixtures encountered in the various chemical engineering and biotechnology industries, and blood. Describing the rheological and transport properties of dilute and concentrated suspensions of

such particles has been a problem of long-standing interest, and has been tackled on a number of occasions using a variety of experimental, analytical and computational methods (Batchelor 1974).

Over the last two decades, significant improvements in the efficiency of computational methods for solving the equations of Stokes flow in the presence of a multitude of compact rigid boundaries, which in the present context may be identified with the surfaces of suspended particles, have allowed the extensive investigation of the rheological and transport properties of a variety of liquid–solid systems, incorporating the effects of Brownian motion (Barnes, Edwards & Woodcock 1987; Brady & Bossis 1988; Kim & Karrila 1991; Roco 1993). Recent examples include numerical simulations of the motion of monodisperse and bidisperse suspensions of spherical and spheroidal particles at various relative volume fractions (Claeys & Brady 1993; Chang & Powell 1993, 1994*a*,*b*). These numerical investigations have illustrated the physical mechanisms that govern the dynamics of the microstructure, established the relationship between the effective rheological properties and the state of the microstructure, and provided a basis for describing the motion of the suspended entities in the context of statistical mechanics.

Much less work has been done on the more challenging problem of suspensions of deformable particles, such as liquid drops with isotropic interfacial tension and deformable capsules enclosed by membranes with generalized mechanical properties. Whereas the mathematical framework for quantifying the effective rheological properties of such suspensions has been established in an unambiguous manner (Batchelor 1974), and the behaviour in the limit of infinite dilution has been addressed successfully on a number of occasions and for a variety of interfacial constitutions (Pozrikidis 1995), difficulties in computing Stokes flow in the presence of a multitude of deforming boundaries have prevented the study of non-dilute systems with strong hydrodynamic interactions. Fortunately, in the limit of high volume fractions, certain types of motion can be described on essentially geometrical grounds using simplified models of foam that employ the theory of lubrication flow (Reinelt & Kraynik 1990; Li, Zhou & Pozrikidis 1995). It is perhaps ironic that the corresponding limit of maximum packing for suspensions of rigid particles is more difficult to analyse owing to the paramount importance of lubrication forces, as manifested by the fact that the rate of viscous dissipation at the points of minimum separation obtains large values (Frankel & Acrivos 1967). Assuming that a suspension has a spatially periodic structure renders the computational problem tractable, at the expense, however, of generality and physical relevance (Pozrikidis 1993).

At high volume fractions, the motion of a suspension of liquid deformable particles differs from that of solid particles in two fundamental ways. First, liquid particles with mobile interfaces and moderate viscosity are able to pass each other without much resistance. They may thus be contrasted with solid particles which tend to adhere to each other for a long period of time owing to the strong lubrication forces, forming long-lived clusters. Second, deformable particles with structured interfaces, such as capsules enclosed by elastic membranes, negotiate collisions by changing their shape as they move past their neighbours, and this results in higher effective mobilities. Thus, although a solitary spherical capsule enclosed by an elastic membrane rotates nearly as a rigid body in simple shear flow, its trajectory during collision with another capsule is significantly different from that of a rigid particle owing its ability to deform at close contact. Interfacial mobility and particle deformability work synergistically to make a suspension capable of accommodating externally imposed strains with a relatively small resistance.

In previous studies, we investigated the motion of suspensions of two-dimensional liquid drops with uniform surface tension in a channel that is confined by two parallel walls, by means of dynamic simulations (Zhou & Pozrikidis 1993*a*,*b*, 1994). Appreciable computational cost, required for the computation of the pertinent Green's function of Stokes flow, prevented us from studying the motion of random systems with more than twelve drops per periodic cell, and thus from carrying out a meaningful analysis of the motion using methods of statistical mechanics. Furthermore, the presence of walls introduced spatial inhomogeneities that render the results inapplicable to spatially homogeneous systems. For example, it was observed that the drops show a strong tendency to migrate away from the walls, and this prevents the drops that are located close to the centreline of the channel from travelling a significant distance away from their initial positions.

In the present paper, we study the motion of unbounded, random suspensions of liquid drops with uniform surface tension in a doubly-periodic arrangement. Our primary objective is to identify the salient differences from the analogous motion of suspensions of rigid particles studied by previous authors, concerning the rheological properties and the dynamics of the microstructure. The idealization of two-dimensional motion, motivated by computational cost alone, appears to be an acceptable compromise for dense systems where issues of ill-posedness of two-dimensional Stokes flow do not arise; experience has shown that the similarities between three-dimensional and two-dimensional Stokes flow outweigh their differences. For example, the radial equilibrium pair-distribution function of hard spheres arranged in a plane, defined in § 3 of this paper, is identical to that of hard disks (Bossis & Brady 1987), and the tensions developing around two-dimensional capsules with incompressible interfaces are similar to those developing around their three-dimensional counterparts (Zhou & Pozrikidis 1995). One may thus expect with confidence that the statistical properties of the motion of three-dimensional drops arranged in a plane will be similar to those of the two-dimensional drops considered in the present study.

An additional assumption adopted in the present study, also motivated by considerations of computational cost, is that the viscosity of the drops is equal to that of the ambient fluid. As the viscosity of the drops is raised, the behaviour of the drops tends to resemble that of solid particles, and this suggests that the viscosity ratio is indeed a significant parameter of the motion. The motion for equal viscosities, however, is typical of that of drops whose viscosity is roughly less than four times that of the ambient fluid (Kennedy, Pozrikidis & Skalak 1994; Stone 1994).

The present dynamic simulations are conducted using the method of interfacial dynamics, which is an advanced implementation of the boundary integral method for Stokes flow. The numerical procedure involves two new features that drastically reduce the cost of the computations and make extensive parametric investigations feasible: the use of interpolation tables for computing the doubly periodic Green's function, and the implementation of the method of multipole expansion to account for remote drop interactions.

2. Problem statement and numerical method

Consider the motion of a doubly periodic monodisperse suspension of neutrally buoyant two-dimensional liquid drops with viscosity μ and uniform surface tension γ, suspended in an ambient fluid with identical viscosity. The arrangement of the drops is repeated periodically along the x- and y-axes with periods equal to L, as

shown in figure 1(*a–d*). The suspension executes simple shearing motion along the x-axis as follows. In the absence of the drops, or when the surface tension vanishes, the unperturbed velocity field is given by $\boldsymbol{u}^{\infty} = (ky, 0)$, where k is the constant shear rate. The shear flow causes the drops to translate and deform thus generating a perturbation flow due to the surface tension. The flow rate associated with the perturbation velocity field along the x- or y-axis is required to vanish at all times.

The geometry of the doubly periodic array can be described by two material vectors $\boldsymbol{a}_1$ and $\boldsymbol{a}_2$ that evolve under the action of the unperturbed shear flow. At the initial instant, $\boldsymbol{a}_1$ and $\boldsymbol{a}_2$ are oriented along the x- and y-axes and have identical lengths equal to L. Any one or both of $\boldsymbol{a}_1$ and $\boldsymbol{a}_2$ may be replaced with any of their linear combinations at any time.

At the initial instant, each periodic box contains N randomly distributed non-overlapping circular drops of radius equal to a. The area fraction of the suspended phase is thus equal to $\phi = N\pi a^2/L^2$. The maximum area fraction for randomly distributed non-overlapping circular disks has been determined to be 0.82 (Kausch, Fesko & Tschoegl 1971); this value lies between the maximum value for circular disks arranged on a square lattice at close packing, which is equal to 0.785, and that for circular disks arranged on a hexagonal lattice at close packing, which is equal to 0.907. In the simulations reported in this paper, we consider the motion for two values $\phi = 0.10$ and 0.40 representing a dilute and a dense system, respectively.

Non-dimensionalizing all variables using as length scale the equivalent drop radius a and time scale the inverse shear rate $1/k$, we find that the motion of the suspension depends upon the number of drops per periodic box N, the area fraction ϕ, the drop capillary number $Ca = \mu ka/\gamma$, and the distribution of the drops at the initial instant. The results of the present simulations, as well as those of previous authors for solid particles, suggest that the initial drop distribution is not statistically significant when N is sufficiently large, roughly more than 20. An exception arises in the computation of the long-time self-diffusivity, which requires larger values of N.

2.1. *Boundary integral formulation*

When the Reynolds number Re based on the shear rate k and the equivalent drop radius a is small, $Re = ka^2/\nu \ll 1$, where ν is the kinematic viscosity of the fluid, the flow inside and outside the drops is governed by the continuity equation

$$\nabla \cdot \boldsymbol{u} = 0 \tag{2.1}$$

and the Stokes equation

$$-\nabla p + \mu \nabla^2 \boldsymbol{u} + \rho \boldsymbol{g} = 0, \tag{2.2}$$

where ρ and μ are the density and the viscosity of the drop or of the ambient fluid. Following the standard boundary integral formulation for Stokes flow, we express the velocity as the sum of the incident velocity $\boldsymbol{u}^{\infty}$ and a single-layer potential due to the discontinuity in traction across the interfaces $\Delta \boldsymbol{f}$,

$$u_j(\boldsymbol{x}_0) = u_j^{\infty}(\boldsymbol{x}_0) - \frac{1}{4\pi\mu} \sum_{m=1}^{N} \int_{S_{D_m}} \Delta f_i(\boldsymbol{x}) G_{ij}^{DP}(\boldsymbol{x}, \boldsymbol{x}_0)\, \mathrm{d}l(\boldsymbol{x}) \tag{2.3}$$

where S_{D_m} is the interface of the mth drop in a periodic box, $\Delta \boldsymbol{f} = \gamma \kappa \boldsymbol{n}$ is the discontinuity in the interfacial traction, κ is the curvature of the interface in the (x, y)-plane, and $\boldsymbol{n}$ is the unit vector normal to the interface pointing into the ambient fluid (Pozrikidis 1992, Chapter 5). Equation (2.3) is valid both inside and outside the drops as well as at the interfaces. The assumption that the viscosity of the drops

is equal to that of the ambient fluid has allowed us to obtain the velocity simply by computing line integrals, instead of solving a Fredholm integral equation of the second kind, as would be required in the general case.

One important component of the boundary integral representation (2.3) is the Green's function $\mathbf{G}^{DP}(\boldsymbol{x}, \boldsymbol{x}_0)$ representing the doubly periodic flow due to a two-dimensional periodic lattice of point forces with base vectors $\boldsymbol{a}_1$ and $\boldsymbol{a}_2$; one of the point forces is situated at the point $\boldsymbol{x}_0$. The superscript ^{DP} stands for *doubly periodic*. Details on the derivation and numerical computation of $\mathbf{G}^{DP}$ in terms of Ewald sums with terms that decay in a Gaussian manner are given by Pozrikidis (1996*a*). We note, in particular, that the terms within the sum in real space involve the exponential integral which is evaluated using polynomial or rational approximations (Abramowitz & Stegun 1972, p. 231).

2.2. *Numerical method*

The numerical procedure is similar to that used by Li *et al.* (1995) in their study of foam flow, with the addition of the multipole expansion option and the use of interpolation on tables for computing the periodic Green's function. Briefly, we describe the interface of each drop using a set of marker points, and approximate its shape using cubic splines. In a simple implementation of the method, we use as independent interpolating variable the arclength of the polygonal line that connects successive marker points. In a more advanced implementation, we use the arclength of the cubic splines that are computed using the simple method. At each time step, we adjust the distribution of marker points by adding new points or removing existing points so as to (i) maintain the distance between two neighbouring marker points within preset maximum and minimum thresholds, and (ii) maintain the magnitude of the angles subtended by the circular arcs that connect three successive points below another threshold value. A typical computation begins with sixteen points around each interface and ends with thirty points. To advance the position of the marker points, we use the second-order Runge–Kutta method, and in some cases the third-order Runge–Kutta–Fehlberg method (RKF23). The latter is necessary at the high area fraction and small capillary numbers where numerical error may lead to artificial drop coalescence. The error due to the temporal integration was found to cause an average cumulative change of 4% in the area of the suspended phase during the course of a simulation from $kt = 0$ up to $kt = 60$.

The computation of the velocity at each one of the K marker points requires evaluating the Green's function at least K times, and this results in a prohibitive computational cost. To circumvent this difficulty, we implemented two independent but not mutually exclusive options.

First, to evaluate the velocity at a point that is located sufficiently far from a particular drop interface and its periodic repetitions, we replace the boundary integral over that drop with the velocity due to a point-force dipole located at the centre of mass of the drop. This is done by considering the disturbance velocity due to the mth drop in the periodic lattice, which is given by

$$u_j^{D_m}(\boldsymbol{x}_0) = -\frac{1}{4\pi\mu} \int_{S_{D_m}} G_{ji}^{DP}(\boldsymbol{x}_0, \boldsymbol{x}) \Delta f_i(\boldsymbol{x}) \, \mathrm{d}l(\boldsymbol{x}). \tag{2.4}$$

Assuming that the marker point $\boldsymbol{x}_0$ is located sufficiently far from the mth interface and its doubly periodic images, we expand the Green's function within the integral

in (2.4) in a Taylor series with respect to the point $\boldsymbol{x}$ about the drop's centre of mass $\boldsymbol{x}_c$, and obtain the multipole expansion

$$u_j^{D_m}(\boldsymbol{x}_0) = -\frac{1}{4\pi\mu} G_{ji}^{DP}(\boldsymbol{x}_0, \boldsymbol{x}_c) \int_{S_{D_m}} \Delta f_i(\boldsymbol{x})\, \mathrm{d}l(\boldsymbol{x}) - \frac{1}{4\pi\mu} \frac{\partial G_{ji}^{DP}(\boldsymbol{x}_0, \boldsymbol{x}_c)}{\partial x_k} \int_{S_{D_m}} (\boldsymbol{x} - \boldsymbol{x}_c)_k \Delta f_i(\boldsymbol{x})\, \mathrm{d}l(\boldsymbol{x}) + \cdots \tag{2.5}$$

(Pozrikidis 1992, Chapter 2). Since each interface is in dynamic equilibrium, the integral in the first term on the right-hand side of (2.5) vanishes. Ignoring the higher-order multipoles represented by the dots, we obtain an expression for the disturbance velocity that is identical to that due to a Green's function dipole whose strength is equal to the second integral on the right-hand side of (2.5). In the numerical procedure, we compute the Green's function dipole from the Green's function using central differences. Furthermore, we use the definition $\Delta \boldsymbol{f} = \gamma \kappa \boldsymbol{n}$ to recast the coefficient of the dipole in the form $\gamma \int_{S_{D_m}} t_k t_i \, \mathrm{d}l$.

To assess the error due to the multipole expansion, we considered a model suspension consisting of two elliptical drops with aspect ratio equal to 2, oriented at an angle of 45° with respect to the x-axis within each periodic box, and carried out several series of tests. In one series, we progressively increased the equivalent drop radius a, while keeping the separation between their centres d constant, and recorded the velocity components as computed by the multipole expansion or with the full interfacial integral. The maximum value of the relative error of both components of the perturbation velocity was found to be less than 5% when d/a was larger than 5.0; the corresponding average value of the relative error was found to be less than 2.5%. Accordingly, when the multipole expansion was enabled, it was allowed to operate only for drops whose separation, or that between their periodic images, was at least five times their equivalent radius. The zone of influence of the multipole expansion for a typical case is shown in figure 1(*a*) with circles. Numerical experimentation showed that the shapes of the drop contours computed using this method were visually indistinguishable from those computed in terms of all interfacial integrals; the computational cost, however, is reduced by a factor of at least 2 (Charles 1996).

A drastic reduction in the cost of the computations is achieved by evaluating the Green's function using trilinear interpolation from custom-made tables. To construct these tables we note that the two components of the vector $(\boldsymbol{x} - \boldsymbol{x}_0)/L$ and a_{21}/L, where a_{21} is the x-component of the base vector $\boldsymbol{a}_2$, vary in the range between zero and unity. We subtract off the two-dimensional Stokeslet, and tabulate the remaining part of the Green's function over a unit cubic box as a function of these variables. The maximum absolute error due to the interpolation was determined to be of order 10^{-5} over the whole domain of the independent variables. The size of the three-dimensional tabulation array necessary to achieve this level of accuracy was $129 \times 65 \times 129$. With the vectorized FORTRAN code, we obtain a reduction in CPU time by a factor of one thousand with respect to that required for the direct evaluation of the Green's function in terms of Ewald sums. Since the savings due to the multipole expansion are insignificant compared to those due to the use of interpolation tables, the former was disabled in the majority of the simulations.

2.3. *Summary of simulations*

We carried out two main series of simulations, one at the low area fraction $\phi = 0.10$, and the second at the higher area fraction $\phi = 0.40$. The initial positions of the

centres of the drops were determined using the standard random-number generator installed on the CRAY C90. If the drops happened to overlap, the configuration was rejected and a new selection was made. The same initial configuration was used in computations with the same value of ϕ and N but different values of Ca. Furthermore, the initial positions of the centres of the drops at the low area fraction were identical to those at the high area fraction, but the radius of the drops was reduced by the required proportion.

The majority of the simulations were performed with 25 drops per periodic box, but a limited number of simulations were carried out with 49 drops. The rheological properties of the suspension and statistical properties of the microstructure exhibited small differences. The effective diffusivity, however, showed slow convergence as discussed in § 5.

A simulation with 25 drops from $kt = 0$ up to $kt = 60.0$ on the CRAY C90 computer of the San Diego Supercomputer Center typically required 1 to $3\frac{1}{2}$ hours of CPU time depending upon the area fraction, capillary number, and time-integration method. The capillary number affects the number of marker points around each drop through the adaptive marker point distribution method. A corresponding computation with 49 drops required nearly 10 hours of CPU time.

3. Drop motion and deformation

The results of the simulations showed that the drops translate, rotate, elongate, and deform as they interact under the action of the simple shear flow, in a manner that depends strongly upon the drop capillary number and area fraction. The results reported in the present and in the subsequent sections correspond to capillary numbers that are low enough so that the drops remain intact and do not suffer excessive elongation or breakup at any time during the motion. The spatial distribution of the centres of the drops appears to be random at all times. Furthermore, all geometric and hydrodynamic variables appear to become stationary random functions after a period of time that is typically equal to $kt = 4$; and this allows us to analyse the motion using methods of statistical mechanics.

Four typical instantaneous configurations of the suspension at the low area fraction $\phi = 0.10$, and the higher area fraction $\phi = 0.40$, with 49 drops per cell, at two capillary numbers, are shown in figure 1(*a–d*). Computer graphics animations for the higher area fraction revealed the formation of transient polygonal structures with several participating drops. The straight lines in figure 1(*d*) connect the centres of drops that appear to belong to clusters. To demonstrate the significant effect of the capillary number and hence of the interfacial deformability, in figure 1(*e*) we have plotted with solid and broken lines the interfaces of drops that evolved from the same initial configuration but with different capillary numbers. The differences are significant.

3.1. *Relative-position pair distribution function*

The state of the microstructure of a suspension of rigid spherical particles can be described by the pair distribution function $g(r, \theta)$. To define this quantity, we consider the probability that the centre of a particle is located within a small area of radial and angular size equal to $\mathrm{d}r$ and $\mathrm{d}\theta$ around the point (r, θ), while the centre of a chosen test particle is centred at the origin. To obtain $g(r, \theta)$, we divide this probability by the particle number density, that is, the average number of particles per unit area of the suspension. As r/a tends to infinity, g tends to obtain the value of unity. The

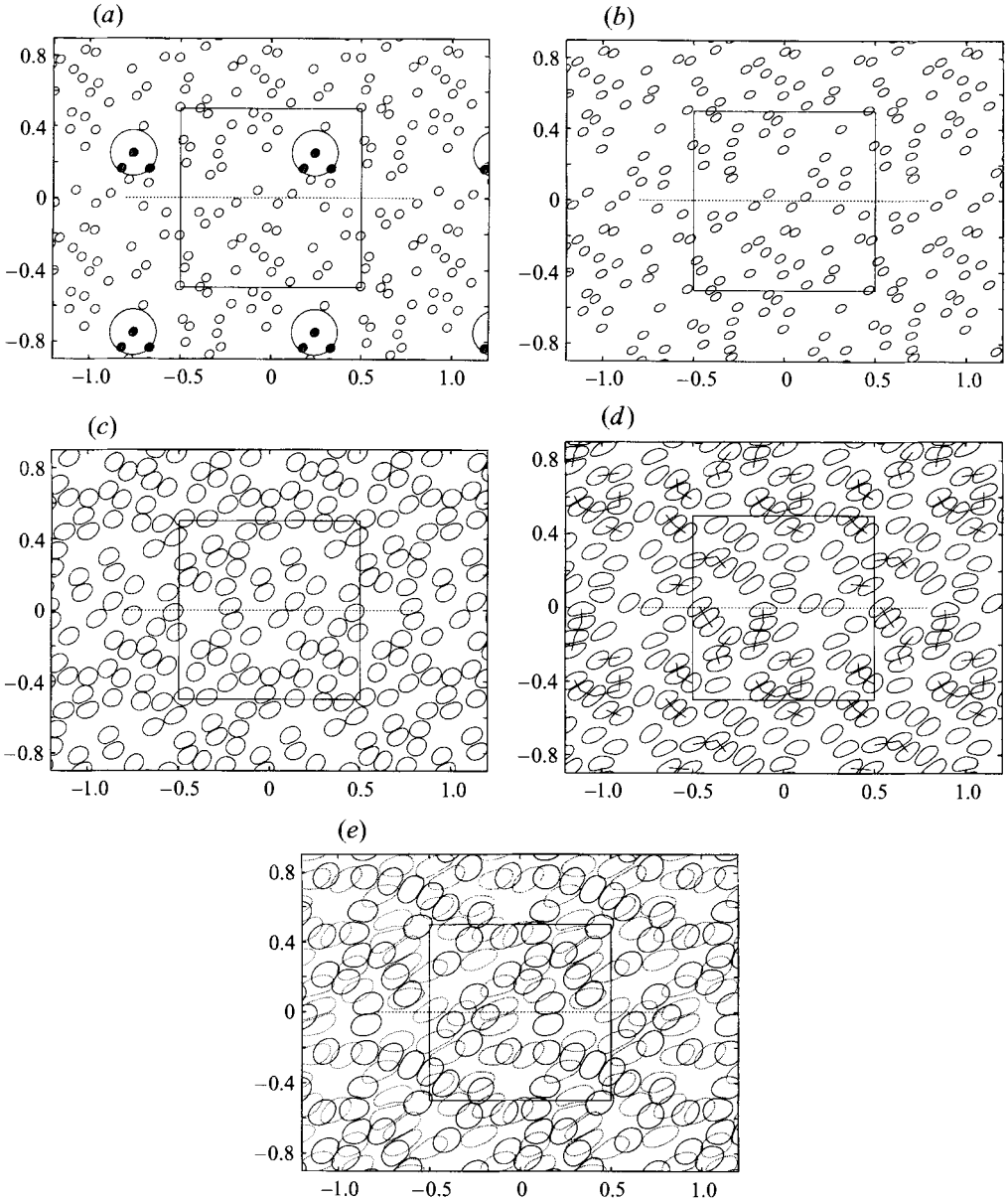

FIGURE 1. Typical instantaneous configurations of a suspension with 49 liquid drops in each periodic box at (*a*) $\phi = 0.1, Ca = 0.08, kt = 10$; the circles show the zone of influence of the multipole expansion; (*b*) $\phi = 0.1, Ca = 0.233, kt = 10$; (*c*) $\phi = 0.4, Ca = 0.08, kt = 10$; (*d*) $\phi = 0.4, Ca = 0.233, kt = 10$; the centres of drops that belong to a cluster are connected by straight lines. (*e*) Comparison between the instantaneous drop interfaces for $\phi = 0.4, N = 25, kt = 40$ at $Ca = 0.08$ (solid) and 0.233 (dotted), showing the effect of interfacial deformability. The suspensions have identical configurations at the initial instant.

integral of $g - 1$ over the whole area of the suspension is a constant equal to zero at all times.

The usefulness of $g(r, \theta)$ is two-fold. First, as explained by Batchelor (1974), knowledge of this function is a prerequisite for computing the second-order contribution

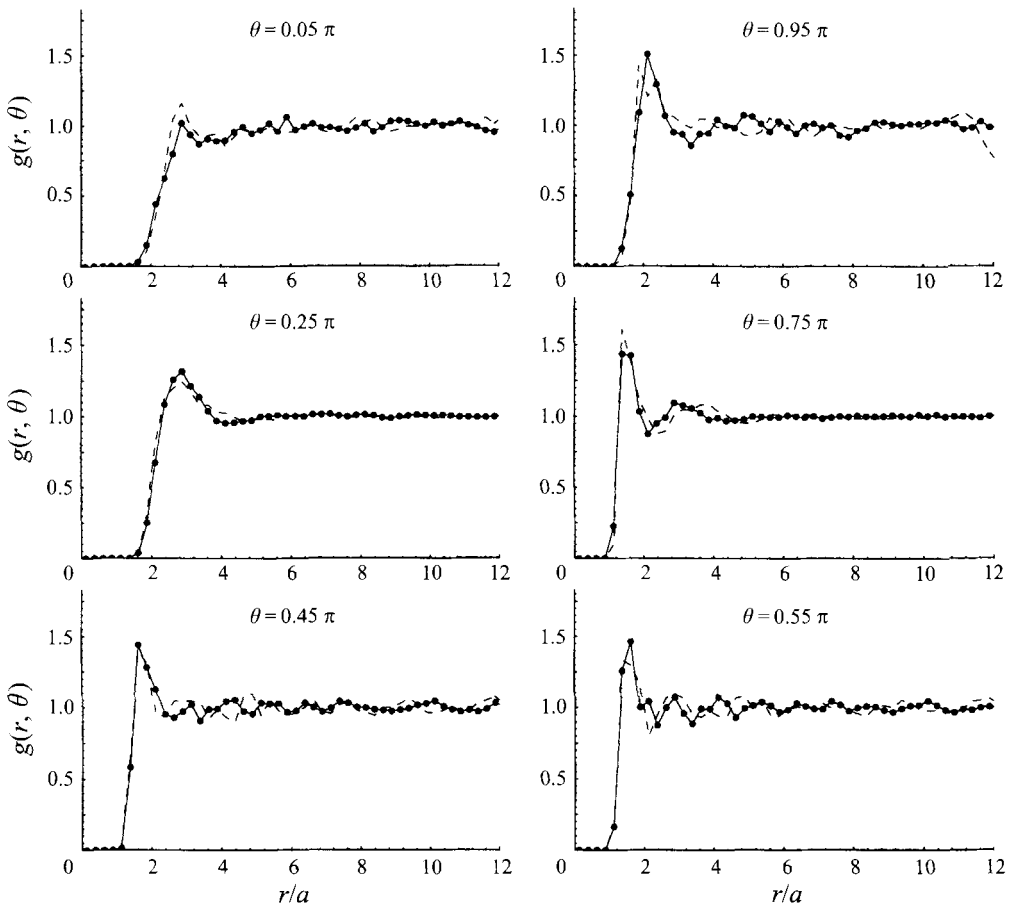

FIGURE 2. Graphs of the pair distribution function $g(r,\theta)$ as a function of radial distance r/a, where a is the equivalent drop radius, for $\phi = 0.4, Ca = 0.233$ at six selected values of the relative angular position measured in the counter-clockwise sense, $\theta/\pi = 0.05, 0.25, 0.45, 0.55, 0.75, 0.95$. The solid lines correspond to numerical simulation with $N = 49$, and the dashed lines correspond to $N = 25$.

of the suspended-phase volume fraction to the effective rheological properties of the suspension. Second, in order to perform Monte Carlo statistical simulations with randomly distributed particles, one must know the statistics of the particle centre distribution which is expressed by the probability density function of the whole configuration space. A minimal amount of relevant information is carried by the pair-distribution function $g(r,\theta)$. Brady & Bossis (1985), Ladd (1990), and Chang & Powell (1993, 1994*a*,*b*) conducted dynamic and Monte Carlo simulations with suspensions of hard spheres, and found significant differences in the effective rheological properties when the particles are distributed in statistically different ways. As the particle distribution becomes uniform, the effective viscosity of the suspension decreases owing to the absence of particle clusters.

In figure 2 we present a typical graph of $g(r,\theta)$ with respect to r/a at six selected values of θ for $\phi = 0.40$, and $Ca = 0.233$. In these computations, we used $\mathrm{d}r/a = 1/4$ and $\mathrm{d}\theta = \pi/10$. The solid lines correspond to $N = 49$ and the dashed lines to $N = 25$; the good qualitative agreement indicates that the latter is sufficient for describing the state of the microstructure.

For monodisperse suspensions of spherical rigid particles of radius a, the domain of definition of $g(r,\theta)$ with respect to radial distance r/a extends between 2 and infinity; the lowest value corresponds to the mathematical but physically unattainable limit of perfect contact. For monodisperse suspensions of deformable particles with effective radius equal to a, $g(r,\theta)$ may take finite values even when r/a is substantially lower than 2, reflecting interfacial deformations at near particle contact. The minimum value of r/a where g is non-zero at a given time, denoted by $\hat{r}_{min}$, is a function of the magnitude of the interfacial deformations and therefore depends on the capillary number. For the conditions corresponding to figure 2, the results show that $\hat{r}_{min}$ can be as low as unity. Further simulations showed that $\hat{r}_{min}$ decreases as the capillary number is raised, but it does not fall below the value of unity. Lower values require that the drops exhibit excessive elongation to the extent that the interfaces do not remain intact.

Brady & Bossis (1988) found that the radial dependence of $g(r,\theta)$ for dense monodisperse suspensions of rigid spherical particles of radius a, at a single value of θ or averaged over the range of θ, shows two sharp maxima at radial distances that are integral multiples of the particle diameter. This indicates cluster formation with two or three adjacent particles aligned in a certain direction on a straight line. Figure 2 reveals the occurrence of a sharp peak at about $r = 2a$ for almost all values of θ except near $\theta = 0$, followed by strong fluctuations but no apparent further peaks. The height of the peak reaches a blunt maximum at the angle $\theta = 0.75\pi$ corresponding to the compressive principal direction of the straining component of the incident shear flow. Because deformable particles at near-contact do not necessarily have the same centre-to-centre distance, the peak for liquid drops is broader than that for rigid particles. Similar results are obtained at lower values of the capillary number where the interfaces are significantly less deformed. Consequently, the ability of the drops to bypass or go over each other prevents the formation of clusters with three or more drops aligned in a certain direction. When the area fraction is reduced to $\phi = 0.10$, the heights of the peaks diminish, and the radial distribution of $g(r,\theta)$ becomes nearly flat at all angular positions but $\theta/\pi = 0.05$ and 0.95 where it shows gradual and monotonic growth.

In studying the motion of suspensions of solid spheres in the absence of non-hydrodyna-mic forces, Brady & Bossis (1985) found that the angular dependence of $g(r,\theta)$, at a particular value of r or averaged over a range of r, is weak but significant, and the angular position where $g(r,\theta)$ reaches maximum value depends upon the particle concentration. Physically, their results indicate that, at low volume fractions, two particles in close proximity spend more time aligned with the streamlines of the unperturbed flow; at high volume fractions they spend more time oriented perpendicular to the unperturbed flow. The behaviour at low volume fraction can be explained by considering the motion of two isolated particles in simple shear flow; at high volume fractions, the rotation of two particles around a common centre is hindered by the presence of other neighbouring particles.

Bossis & Brady (1984) found that the angular dependence of $g(r,\theta)$ is sensitive to the presence of repulsive non-hydrodynamic forces. The action of such forces promotes the angular variation of $g(r,\theta)$ so that the particle concentration is reduced at the downstream location of a reference sphere corresponding to $0 < \theta < \pi/2$, and raised at the upstream side corresponding to $\pi/2 < \theta < \pi$. Physically, the shear stresses on the upstream side push two particles together while the repulsive forces are trying to keep them apart. On the downstream side, both forces act to separate the particles.

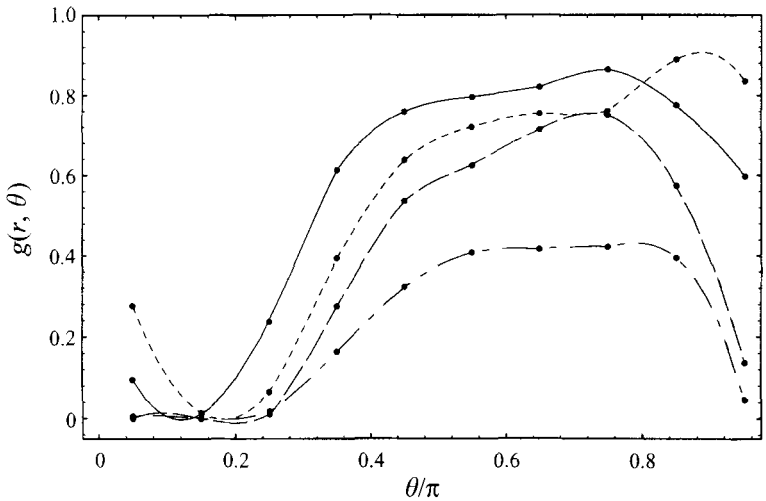

FIGURE 3. The angular dependence of the pair distribution function $g(r,\theta)$, averaged over $r/a < 2.2$, for: ——, $\phi = 0.4, Ca = 0.233, N = 25$; – – –, $\phi = 0.4, Ca = 0.08, N = 25$; – – –, $\phi = 0.1, Ca = 0.233, N = 25$; — — —, $\phi = 0.1, Ca = 0.08, N = 25$.

In figure 3 we plot $g(r,\theta)$ averaged over values of r/a that are less than 2.2, for $\phi = 0.10, 0.40$, and $Ca = 0.08, 0.233$. In all cases, the maximum value occurs at about $\theta/\pi = 0.75$, which shows that the drops spend more time aligned with the compressive principal axis of the shear flow than in any other direction. The gross shape of the curves in figure 3 differs from that of the corresponding curve displayed by Brady & Bossis (1985) at small volume fractions, but is similar to that of the curves presented by Bossis & Brady (1984) for suspensions of spherical solid particles evolving in the presence of non-hydrodynamic interparticle forces. Overall, the present results suggest that interfacial slip and particle deformability play an important role in determining the relative particle distribution.

3.2. *Drop coalescence*

Pairwise and multi-drop interception is a frequent event at high volume fractions. In general, interception of two drops may result in either (*a*) transient orbiting motion accompanied by deformation and followed by bypassing, or (*b*) collision and coalescence. The prevailing behaviour depends upon the initial drop separation, the ability of the interfaces to deform, and the duration of near-contact.

When two spherical non-deformable drops are pushed against each other under the action of a constant force, the interfaces coalesce at a finite time even in the absence of inter-molecular forces (Davis, Schonberg & Rallison 1989). Yiantsios & Davis (1991) demonstrated that allowing for interfacial deformability renders the time required for coalescence infinite and prevents collision. More relevant to the present discussion is the work of Wang, Zinchenko & Davis (1994) who showed that two intercepting spherical drops in simple shear flow may coalesce at a finite time, and computed the rate of collision. Whether interfacial deformability renders the time required for coalescence infinite has not been determined on theoretical grounds, but numerical evidence suggests that it is not likely (Li *et al.* 1995).

In the present simulations, drop collision and small-scale interfacial crossing were observed on occasion at the larger area fraction $\phi = 0.40$ and at the smaller capillary number $Ca = 0.08$ where the drops are nearly circular, when the computations were

conducted using the fixed-time-stepping second-order Runge–Kutta method. Using the adaptive RKF23 method and a finer resolution of the drop interfaces, however, prevented this occurrence.

Li *et al.* (1995) found that a simple shear flow is able to stabilize a densely packed *ordered* suspension of non-circular drops, working against the tendency of surface tension to render the interfaces circular and cause the drops to coalesce in the absence of global expansion. The results of the present simulations suggest a similar behaviour for *random* suspensions: the interfaces separate before they are given a sufficient amount of time to coalesce. Thus, a random emulsion with a large volume fraction, well beyond that corresponding to maximum random packing, resembling a disordered but spatially periodic foam, might be able to survive for a long period of time stabilized by the flow. Confirming the accuracy of this conjecture, however, requires numerical simulations of highly dense random systems, which at the present time are prevented by prohibitive computational cost.

3.3. *Drop deformation and inclination*

In the absence of interparticle hydrodynamic interactions, the drops deform in a similar manner independently of their initial location in the suspension, and the behaviour of the interfaces is determined by the drop capillary number and relative viscosities of the fluids. Under certain conditions the drops are known to deform and reach a stationary state, whereas under other conditions they exhibit continuous rotation with an accompanying oscillation in their aspect ratio. When the viscosity of the drops is equal to that of the ambient fluid, the first type of behaviour prevails.

Weak interparticle interactions cause the drop deformation and inclination to fluctuate around mean values. In figure 4(*a*,*b*) we plot the probability distribution density functions of the drop deformation parameter $D = (A - B)/(A + B)$ and inclination angle α with respect to the x-axis, averaged over a long period of time, $4 < kt < 60$, and over all drops, for a suspension with a low area fraction $\phi = 0.10$ at $Ca = 0.08$. A and B are the maximum and minimum radial distances of the interfaces from the instantaneous centre of the corresponding drop. Both distributions are narrow, with mean values located at approximately $D = 0.094$ and $\alpha/\pi = 0.22$. The solid lines show the Gaussian distributions with identical mean value and standard deviation.

If the drop deformation and inclination angle of each drop in a cell have the same probability distribution, their normalized sum over all drops at a particular instant will be random functions with normal probability density distribution $N(0, 1)$. To test this prediction, in figure 4(*c*) we plot the probability density function of $\zeta_D = \sum_{m=1}^{N}(D_m - \overline{\langle D \rangle})/(\sigma_D N^{1/2})$, where D_m is the deformation for the mth drop in a cell at a certain time, $\overline{\langle D \rangle}$ is the average value over all drops and over all times, and σ_D is the corresponding standard deviation. Similarly, in figure 4(*d*) we present the probability density function of $\zeta_\alpha = \sum_{m=1}^{N}(\alpha_m - \overline{\langle \alpha \rangle})/(\sigma_\alpha N^{1/2})$. The solid lines show the associated Gaussian distribution. Although the fit is not perfect, the results do suggest that the Gaussian distribution may be used with reasonable confidence in a theoretical model.

At moderate and high area fractions, strong interparticle hydrodynamic interactions cause the distributions of the probability density functions of the drop deformation and inclination to spread out away from their mean values. Moreover, the mean values differ substantially from those corresponding to the infinitely dilute system. This behaviour is evident in figure 4(*e*–*h*), which is the counterpart of figure 4(*a*–*d*) for $\phi = 0.40$ and $Ca = 0.233$. We note, in particular, that as the area fraction is

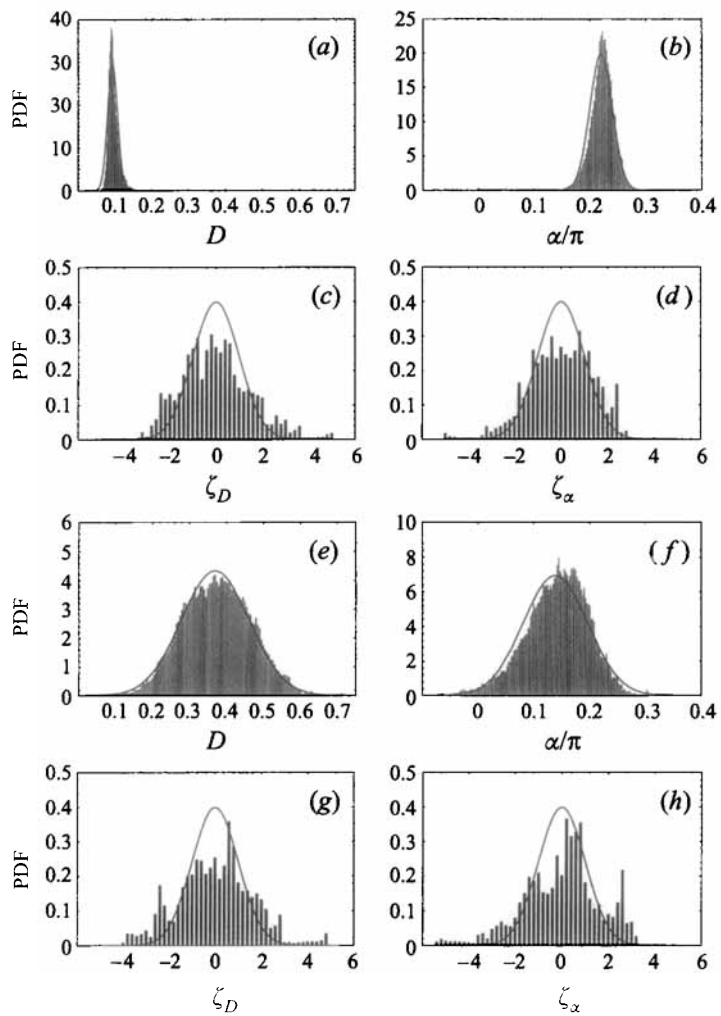

FIGURE 4. (*a*) The probability distribution density function of the drop deformation parameter D, averaged over all drops and over the time period $4 < kt < 60$, for a suspension with $\phi = 0.1, Ca = 0.08, N = 25$.The solid line shows the Gaussian density distribution with identical mean value and standard deviation. (*b*) Same as in (*a*) but for the drop inclination angle α. (*c*) The probability density function for the normalized sum over all drops in a cell at a certain instant, $\zeta_D = \sum_{m=1}^{N}(D_m - \overline{\langle D \rangle})/(\sigma_D N^{1/2})$, where D_m is the deformation for m-th drop and $\overline{\langle D \rangle}$ is the average over time and over all drops. The solid line shows the normal distribution $N(0, 1)$. (*d*) Same as in (*c*) but for the drop inclination angle α. Figures (*e*) to (*h*) are the same as (*a*) to (*d*) respectively but for $\phi = 0.4, Ca = 0.233, N = 25$.

raised, but the drop capillary number is held constant, the mean value of the particle deformation increases, whereas the mean value of the inclination angle is reduced; this means that the drops incline towards the x-axis. The inclination angle of a drop may take negative values with a finite probability, revealing the occurrence of orbiting motions. The mean values of the drop deformation and inclination averaged over all drops and over time are shown in table 1 for several cases.

The pair-distribution functions shown in figures 2 and 3, along with the deformation and orientation distribution functions shown in figure 4, are necessary for carrying

out asymptotic analyses of the rheological properties of the suspensions at low area fractions, or Monte-Carlo-type simulations at high area fractions. For example, in developing a theoretical model, one may approximate the interfacial shapes at small deformations with ellipses described by their inclination and aspect ratio. A knowledge of the statistical distributions of the ellipses' centres, aspect ratio, and inclination are sufficient for studying the motion at low area fractions. At higher area fractions, we also require the probability distribution density functions of the *relative* particle orientation in the whole configuration space. This is defined as the probability that a drop is located at a particular position in space and has a certain orientation, given the fact that another drop is located at the origin and is inclined at a certain angle with respect to the streamlines of the unperturbed shear flow.

In §4 we shall see that a knowledge of the mean values of the drop deformation and orientation *alone* is sufficient for making accurate predictions of the effective instantaneous rheological properties even at high area fractions.

4. Effective rheological properties

When the viscosity of the drops is equal to that of the ambient fluid, the effective stress tensor $\langle \sigma_{ij} \rangle$ is

$$\langle \sigma_{ij} \rangle = -\delta_{ij} \langle P \rangle + 2\mu \langle e_{ij} \rangle + \frac{\gamma}{A} \int_C t_i t_j \, \mathrm{d}l, \tag{4.1}$$

where the line integral is over the interfaces of all drops in a periodic box, $\boldsymbol{t}$ is the unit tangential vector pointing in the counter-clockwise direction around the interfaces, and the brackets denote the average value over the area of one periodic cell (Li *et al.* 1995). Note that the integral in (4.1), called the particle stress tensor, is the coefficient of the dipole discussed in §2. The instantaneous effective shear viscosity μ_{EFF} and normal stress difference $\mathcal{N}_{EFF}$ are then given by

$$\mu_{EFF} = \tfrac{1}{2} \langle \sigma_{12} \rangle / \langle e_{12} \rangle, \quad \mathcal{N}_{EFF} = \langle \sigma_{11} \rangle - \langle \sigma_{22} \rangle. \tag{4.2}$$

Physically, the effective shear viscosity is proportional to the total rate of energy dissipation in the flow, whereas the first normal stress difference is a measure of the elastic properties of the suspension.

A seemingly paradoxical behaviour occurs for circular drops: the off-diagonal integral on the right-hand side of (4.1) vanishes, and this appears to suggest that deformation is necessary for the particle stress tensor to have a finite value. Nearly circular drops, however, require small values of the capillary number. The aforementioned integral scales with Ca and, thus, when it is multiplied by γ, it yields a finite product (Pozrikidis 1993).

The results of the simulations show that μ_{EFF} and $\mathcal{N}_{EFF}$ increase in time from the initial values of one and zero, and then fluctuate around well-defined mean values denoted by $\overline{\mu}$ and $\overline{\mathcal{N}}$. This behaviour is consistent with our earlier remark that the motion reaches a state of dynamic equilibrium and the flow variables become stationary random functions. As an example, in figure 5(*a*,*b*) we plot with solid lines the evolution of the effective viscosity and normal stress difference for a typical case with $\phi = 0.40$ and $Ca = 0.233$.

Before proceeding to discuss the effect of area fraction and capillary number, we consider predicting the rheological properties of the suspension from a knowledge of the geometry of the microstructure. According to (4.1), the shape of the interfaces

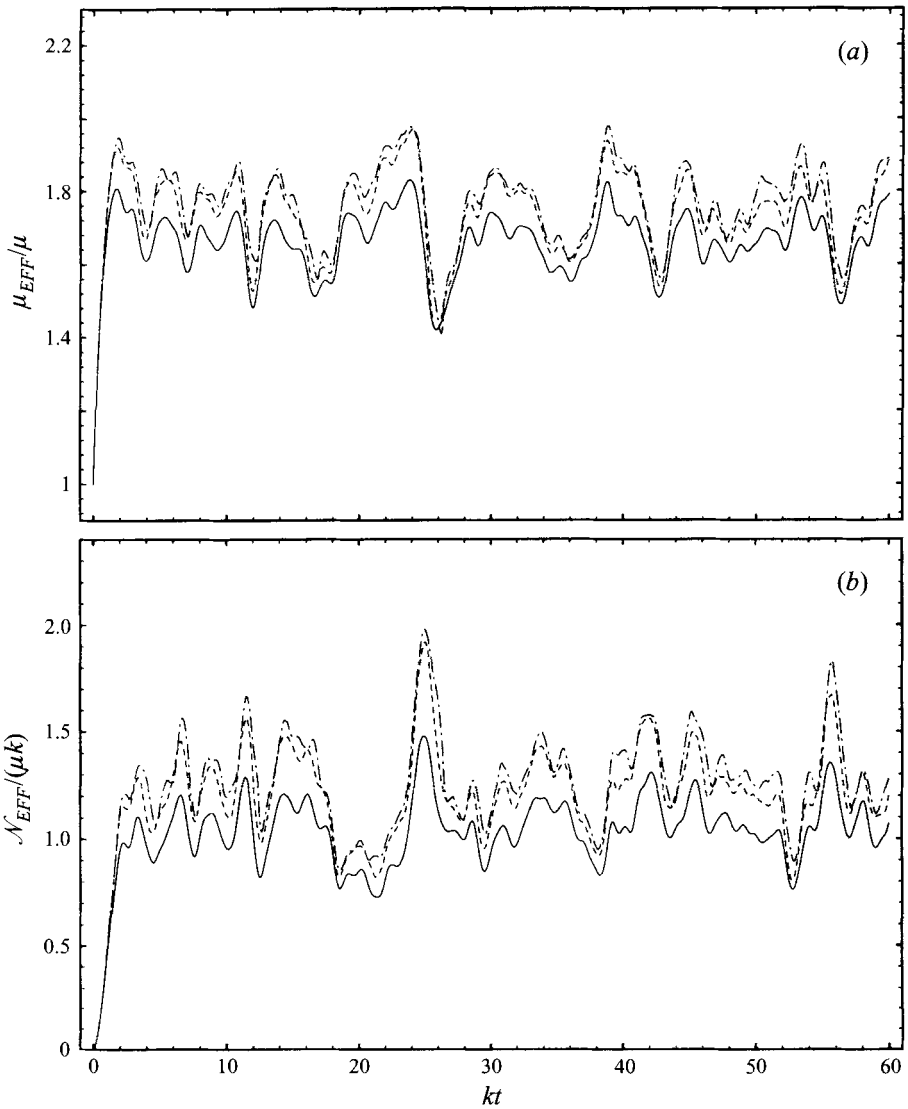

FIGURE 5. (*a*) The evolution of the effective viscosity μ_{EFF} for $\phi = 0.4, Ca = 0.233, N = 25$ (——); the viscosity predicted by replacing each drop with an ellipse of identical deformation D, inclination α, and area (– – –); and that predicted by replacing all drops with the same ellipse corresponding to deformation $\langle D \rangle$ and inclination $\langle \alpha \rangle$ (– – –). (*b*) Same as in (*a*) but for the effective normal stress difference $\mathcal{N}$.

alone is sufficient for computing the particle stress tensor; the instantaneous velocity field is not required. In the simplest possible approximation, we assume that all drops have identical elliptical shapes whose aspect ratio corresponds to a value of the deformation parameter that is equal to $\langle D \rangle$, and are inclined at the same angle $\langle \alpha \rangle$, where the brackets indicate the instantaneous average over all drops. Straightforward analytical computation of the contour integral in (4.1) produces the dot-dashed lines in figure 5(*a*,*b*). The agreement between the actual results and the predictions of the model is remarkably good. The dashed lines in figure 5(*a*,*b*) represent the predictions that arise by assuming that the interfaces have elliptical shapes whose

ϕ	Ca	$\overline{\langle D \rangle}$	$\overline{\langle \alpha \rangle}/\pi$	$\overline{\mu}$	$\overline{\mathcal{N}}$
0.1	0.08	$0.0945 \pm 0.6\times10^{-3}$	$0.2198 \pm 0.3\times10^{-3}$	$1.166 \pm 0.1\times10^{-2}$	$0.0649 \pm 0.7\times10^{-3}$
0.1	0.15	$0.1718 \pm 0.5\times10^{-3}$	$0.1969 \pm 0.7\times10^{-3}$	$1.1574 \pm 0.3\times10^{-3}$	$0.109 \pm 0.2\times10^{-2}$
0.1	0.233	$0.259 \pm 0.3\times10^{-2}$	$0.1710 \pm 0.5\times10^{-3}$	$1.145 \pm 0.2\times10^{-2}$	$0.162 \pm 0.3\times10^{-2}$
0.4	0.08	$0.1681 \pm 0.6\times10^{-3}$	$0.204 \pm 0.2\times10^{-2}$	$2.031 \pm 0.3\times10^{-2}$	$0.61 \pm 0.3\times10^{-1}$
0.4	0.15	$0.272 \pm 0.4\times10^{-2}$	$0.172 \pm 0.2\times10^{-2}$	$1.84 \pm 0.1\times10^{-1}$	$0.86 \pm 0.2\times10^{-1}$
0.4	0.233	$0.371 \pm 0.5\times10^{-2}$	$0.1395 \pm 0.7\times10^{-3}$	$1.668 \pm 0.6\times10^{-2}$	$1.054 \pm 0.9\times10^{-2}$

TABLE 1. Mean values of geometrical and rheological variables.

area, deformation parameter, and inclination are identical to those of the actual drops. The improvement in accuracy is evident but not striking.

The mean values of $\langle D \rangle$ and $\langle \alpha \rangle$ over a long time period $4 < kt < 60$ are listed in table 1 for two area fractions and three values of the capillary number. The quantity listed in each entry of the table was obtained from three different runs with the same area fraction and capillary number but different initial drop distributions.

When the drop capillary number is low enough so that the drops do not break up due to the flow yielding a polydisperse system, $\overline{\mu}$ is known to be a monotonically increasing function of the area fraction; our numerical results are consistent with this experience. For example, as the area fraction increases from 0.10 to 0.40, $\overline{\mu}$ almost doubles from 1.166 to 2.031 for $Ca = 0.08$. There is a critical value of the area fraction above which the drops are not able to accommodate the large interfacial deformations required for passing one another, drop collision occurs, and the drops coalesce. This, however, does not imply that the effective viscosity assumes very large values, as it does for suspensions of rigid particles. Physically, lubrication forces between intercepting rigid particles play a dominant role, and the rate of viscous dissipation tends to diverge, halting the motion of the suspended phase (Frankel & Acrivos 1967). The singular behaviour of the effective shear viscosity of suspensions of rigid spherical particles at the critical volume fraction for maximum random packing has been demonstrated on a number of occasions (Brady & Bossis 1985), but there is no corresponding evidence for suspensions of liquid drops.

In table 1 we collect the average values of the effective viscosity and normal stress difference at low and high area fractions, as functions of the capillary number. Shear-thinning and elastic behaviour are evident especially at the high area fraction; the latter is indicated by the finite values of the normal stress difference. There is a clear correlation between the effective rheological properties and the average drop deformation and orientation at both volume fractions, confirming that drop deformation and tilting are quantities of paramount rheological importance.

4.1. *Significance of clusters*

The effective viscosity of a dense suspension of *rigid* particles is determined, primarily, by the strong lubrication forces associated with cluster formation (Brady & Bossis 1985). Thus, cluster size and orientation are variables of primary importance. For liquid drops with mobile interfaces, it is not clear whether the flow within the narrow gaps between adjacent interfaces makes a dominant contribution to the overall rate of viscous dissipation, although there is numerical evidence that drop aggregation causes the effective viscosity of the suspension to increase by a substantial factor (Zhou & Pozrikidis 1993*b*).

The computation of cluster size in suspensions of rigid spherical particles is carried out by comparing the particle centre-to-centre separation with a preset minimum distance that is typically set equal to 2.02 times the particle radii (Bossis & Brady 1989; Chang & Powell 1994*b*). Owing to significant interfacial deformations, this criterion was found to be inadequate in the present case of deformable drops, as it fails to associate drops whose motion appears to be correlated when viewed in animation. Instead, the association of a drop with a cluster was accomplished by comparing the minimum distance between the interfaces of all pairs of drops. These distances were tested against a threshold value that was set equal to $0.30a$ or $(0.15 + \langle D \rangle)a$, where a is the initial radius of the circular drops. Testing all drops for their positioning with respect to all other drops can be done a systematic way in terms of a *proximity matrix* relating single drop pairs. This matrix is interrogated recursively so that pairwise associations lead to cluster chains (figure 1*d*). When all of the drops have been associated with a cluster chain, the mean cluster size $\langle s \rangle$, defined as the number of drops in a cell divided by the number of clusters, is computed. Figure 1(*d*) shows the cluster pattern identified using the first criterion.

The results of these computations were inconclusive. For example, using the first aforementioned criterion we find that the mean cluster size, averaged over all times, is a decreasing function of the capillary number. However, when the separation of the interfaces was tested against the empirical distance $(0.15+\langle D \rangle)a$, the functional dependence of the mean cluster size on the capillary number was reversed, although the correlation between the instantaneous value of the mean cluster size and effective viscosity became sharper. Thus, cluster formation is not a significant aspect of the motion of liquid drops whose viscosity is lower than or comparable to that of the ambient fluid.

5. Long-time hydrodynamic self-diffusivity

When the position of the centre of a spherical particle in a flowing suspension is sampled over a sufficiently long period of time, the particle appears to execute random motion that is describable in terms of an effective long-time hydrodynamic symmetric self-diffusivity tensor $\boldsymbol{D}$ (Eckstein, Bailey & Shapiro 1977; Leighton & Acrivos 1987; Acrivos *et al.* 1992). When both the suspension and the unperturbed flow are spatially homogeneous, it is reasonable to assume that $\boldsymbol{D}$ is independent of position in the flow, and regard it as a tensorial transport constant. The precise relationship between the magnitude of the self-diffusivity tensor and the effective viscosity or normal stress differences has not been established, apart from the observation that they all tend to increase as the volume fraction is raised. Similar arguments can be made for suspensions of deformable particles and drops in doubly periodic formation considered in the present study.

In previous theoretical and computational studies of simple shear flow along the x-axis, the principal axes of the symmetric diffusivity tensor $\boldsymbol{D}$ have been assumed to be parallel to the x- and y-axes, and the random particle motion was described in terms of the two non-vanishing diagonal terms D_{xx} and D_{yy}. A physical justification for this choice is elusive, although an analogy between particle motion in a suspension and tracer dispersion in a turbulent shear flow, where this assumption has prevailed, could be invoked (Monin & Yaglom 1965, p. 638).

Allowing the principal axes of $\boldsymbol{D}$ to be inclined with respect to the direction of the shear flow renders $\boldsymbol{D}$ non-diagonal. A standard way of computing the components of $\boldsymbol{D}$ is based upon the observation that, if a large number of diffusing point particles are concentrated at the initial position (x_0, y_0) at time t_0, in the presence of the simple

shear flow $u_x = ky + U, u_y = 0$ where U is a constant, then the probability of finding a particle at the position (x, y) at a subsequent time t is identical to the Green's function of the corresponding convection-diffusion equation, which is given by

$$G = \frac{1}{4\pi\hat{t}(D_{yy}\eta)^{1/2}} \exp\left[\frac{(\hat{x} - (\frac{1}{2}k\hat{t} + D_{xy}/D_{yy})\hat{y})^2}{4\eta\hat{t}} - \frac{\hat{y}^2}{4D_{yy}\hat{t}}\right] \tag{5.1}$$

where $\eta = D_{xx} + (k^2\hat{t}^2/12 - (D_{xy}/D_{yy})^2)D_{yy}$, $\hat{x} = x - x_0 - (ky + U)\hat{t}$, $\hat{y} = y - y_0$, and $\hat{t} = t - t_0$ (Chandrasekhar 1943). The second moment of the particle centre deviations from the unperturbed path, corresponding to the variables with the caret, is found directly from the convection-diffusion equation to be

$$\int \hat{x}\hat{x}G \, \mathrm{d}x \, \mathrm{d}y = \begin{bmatrix} 2D_{xx}\hat{t} - 2kD_{xy}\hat{t}^2 + \frac{2}{3}k^2D_{yy}\hat{t}^3 & 2D_{xy}\hat{t} - kD_{yy}\hat{t}^2 \\ 2D_{xy}\hat{t} - kD_{yy}\hat{t}^2 & 2D_{yy}\hat{t} \end{bmatrix} \tag{5.2}$$

(Pozrikidis 1996*b*). Under the ergodic assumption, the left-hand side of (5.2) is replaced by corresponding ensemble averages or instantaneous spatial averages involving the location of the centres of all particles in a certain realization; the latter will be denoted by $\langle\ \rangle$.

In analysing our results, we compute the diffusivities in terms of the products of the modified particle displacement $X(t) = x(t) - x(0) - ky(t)t$ and $Y(t) = y(t) - y(0)$, where $x(t)$ and $y(t)$ designate the coordinates of the centre of a drop. According to (5.2), the diffusivity D_{yy} may be obtained as the limit of

$$D_{yy} = \frac{\langle Y^2(t)\rangle}{2t} \simeq -\frac{\langle X(t)Y(t)\rangle}{kt^2} \simeq \frac{\langle X^2(t)\rangle}{\frac{2}{3}k^2t^3}, \tag{5.3}$$

as t tends to infinity. It should be noted that failure of the three ratios in (5.3) to reach steady values or fluctuate around mean values at large times should be regarded as evidence that the concept of regular hydrodynamic diffusion due to random motion is inappropriate, and a more general dispersion model should be used. The numerical simulations of Bossis & Brady (1987) and Chang & Powell (1994*b*) support the validity of (5.3), and hence corroborate the description of the motion of solid spherical particles in terms of regular diffusion.

In figure 6(*a*) we plot the three ratios defined in (5.3) for $N = 25$, $\phi = 0.40$, and $Ca = 0.233$, and obtain three curves that appear to tend to the same asymptotic limit at long times, which is approximately equal to $0.017ka^2$. Similar computations with a higher number of drops, $N = 49$, or different initial drop-centre distributions, showed that D_{yy} varies between $0.007ka^2$ and $0.022ka^2$. The computed diffusivity is expected to converge as $N^{-1/2}$, and this explains the substantial range of variation. Comparing our results to the corresponding result of Bossis & Brady (1987) and Chang & Powell (1994*b*) for suspensions of solid spheres, we find that the diffusivity of deformable particles is lower than that of solid spheres at the same volume fraction, by a factor as large as 5.

Similar results were obtained for the lower area fraction. Figure 6(*b*) illustrates the behaviour of the three ratios for $N = 25$, $\phi = 0.10$, and $Ca = 0.233$. The three curves appear to fluctuate around the mean value $0.004ka^2$, although the amplitude of the fluctuation is large.

Concentrating on the behaviour at small volume fractions, we examine the numerical results with reference to asymptotic predictions. At infinite dilution, spherical rigid particles or liquid drops move along straight paths, and the particle diffusivity vanishes. Leighton & Acrivos (1987) found that, for monodisperse suspensions of

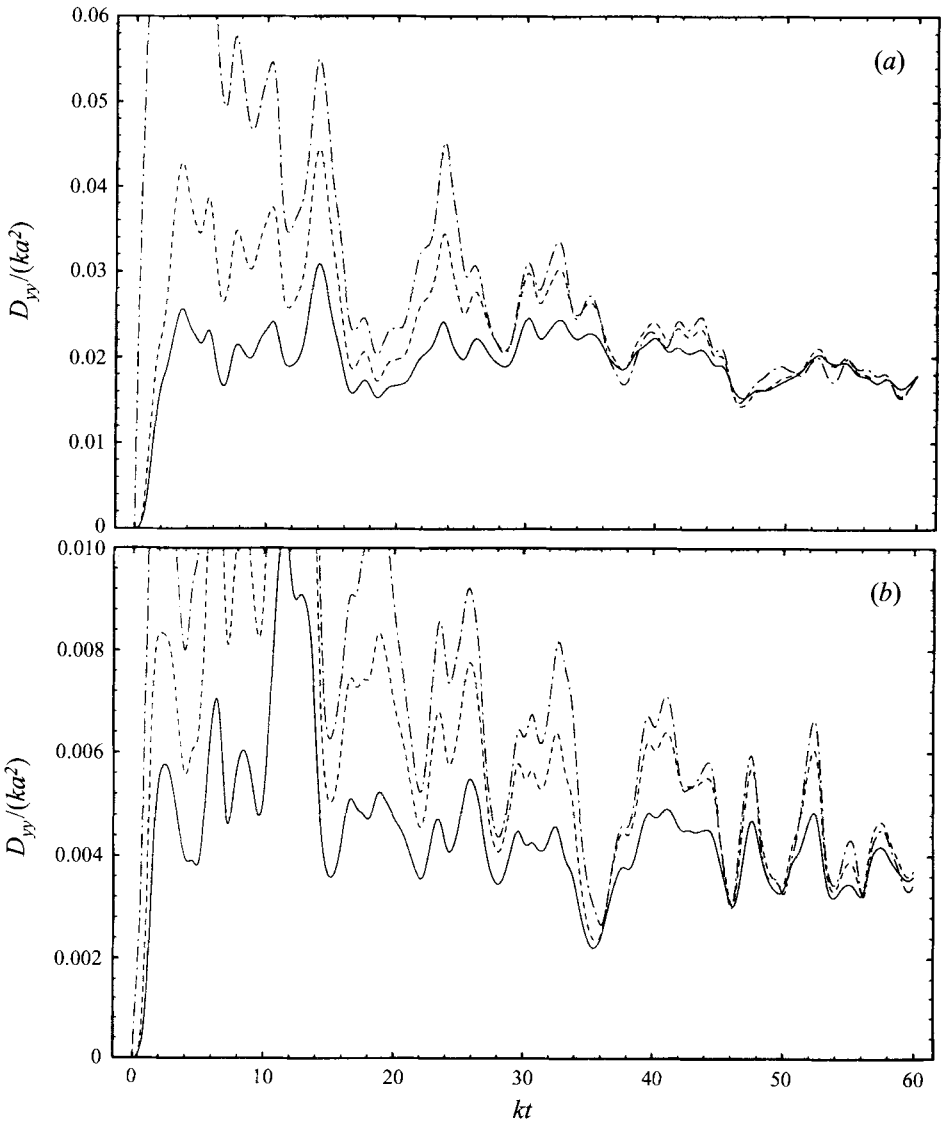

FIGURE 6. (*a*) The dimensionless diffusivity $D_{yy}/(ka^2)$ obtained from the three ratios defined in equation (5.3) as a function of time for $\phi = 0.4, Ca = 0.233, N = 25$: ——, $\langle Y^2(t)\rangle/(2kta^2)$; – – –, $-\langle X(t)Y(t)\rangle/(k^2t^2a^2)$; – · –, $\langle X^2(t)\rangle/(\frac{2}{3}k^3t^3a^2)$. (*b*) Same as in (*a*) but for $\phi = 0.1, Ca = 0.233, N = 25$.

spherical solid particles of radius a, D_{yy} behaves like $0.5ka^2\phi^2$. Acrivos *et al.* (1992) pointed out that occasional hydrodynamic interactions among three particles are necessary in order to prevent D_{xx} from diverging due to pairwise interactions, and deduced the asymptotic form $D_{xx} \sim 0.267ka^2\phi \ln(1/\phi)$.

Reversibility of Stokes flow requires that two intercepting spherical particles interacting in isolation under the influence of a simple shear flow do not exhibit a net displacement after separation, and this explains the aforementioned quadratic dependence of D_{yy} on ϕ. Deformable particles, on the other hand, do exhibit a net displacement whose magnitude depends upon their initial position and capillary number. Using standard arguments of diffusion due to random walk, we find that

D_{yy} scales with $ck(\Delta y)^2\phi$, where c is a dimensionless constant, and Δy is the typical magnitude of the net displacement.

To estimate the magnitude of Δy, we performed a series of simulations with two drops within each periodic box. At the initial instant, the drops were distributed evenly along the x-axis, and were displaced up or down in an alternating manner by the distance ϵa. For $Ca = 0.233$, we found that $\Delta y/a$ varies from 0.42 and 0.59 as ϵ ranges between 0.25 and 0.50. A knowledge of the range of variation of $\Delta y/a$ allows us to estimate the magnitude of the aforementioned constant c. Taking $\Delta y/a = 0.50$, we find that c is approximately equal to 0.16 for both volume fractions, and this shows that the linear dependence of the diffusivity on the volume fraction persists at large volume fractions.

Chang & Powell (1994*b*) computed the diffusivity of monodisperse suspensions of rigid spherical particles at low volume fractions. At $\phi = 0.10$, they found that $D_{yy}/(ka^2)$ is roughly equal to 0.002, and this is substantially smaller than our value of 0.004. It is clear that the diffusivity of deformable particles at low volume fractions is higher than that of solid spheres; and this is consistent with the respective linear or quadratic dependence on ϕ.

Interfacial deformation reduces the relative displacement of two intercepting drops by permitting them to accommodate each other via deformation instead of lateral motion. One might thus argue that particle deformability reduces the value of the lateral hydrodynamic diffusivity. On the other hand, interfacial deformability is known to enhance the migration of a drop away from a boundary, resulting in higher displacements from the unperturbed path. This observation would appear to suggest that, as the capillary number is raised while all other parameters are kept constant, the diffusivity tends to obtain higher values, at least when the suspension is dense. Our numerical results show that $D_{yy}/(ka^2) = 0.021 \pm 0.003$ when $Ca = 0.08$ and $D_{yy}/(ka^2) = 0.014 \pm 0.008$ when $Ca = 0.233$ at $\phi = 0.40$. These values clearly demonstrate that as Ca is raised and the interfaces tend to undergo more severe deformations the diffusivity is reduced. The effect of the capillary number on the particle diffusivity at low area fractions could not be assessed to satisfaction owing to numerical uncertainties.

The computation of the longitudinal and cross-diffusivity was prevented by random noise due to the small size of the simulated system. As a result, the orientation of the principal directions of the symmetric part of the diffusivity tensor could not be estimated with confidence.

6. Discussion

The results of the simulations showed that the motion of a random suspension of liquid drops whose viscosities are equal to that of the ambient fluid, in simple shear flow, differs from the motion of suspensions of solid spherical particles studied by previous authors in several fundamental ways.

In the case of drops, interfacial mobility prevents the particles from lining up to form linear chains, and a percolation-like transition is not observed at a critical area fraction. Instead, we observe the formation of loosely defined structures with a few participating drops. The computation of the cluster size is sensitive to the particular algorithm employed to associate a drop with a cluster, as well as to the specified numerical thresholds. These difficulties render the formation of clusters a secondary mechanism in the rheology of the flow and the dynamics of the microstructure of suspensions of liquid drops.

One of the most striking findings is that a knowledge of the mean particle deformation and orientation is sufficient for estimating the rheological properties of the suspension with a high degree of accuracy, even at high area fractions. This information must be obtained from dynamic simulations and cannot be deduced from Monte-Carlo-type studies.

Furthermore, the results of the dynamic simulations confirmed that the seemingly random motion of the centres of the drops, when viewed at sufficiently long intervals of time, may be described in terms of a self-diffusivity tensor. At high area fractions, the computed value of the lateral component of the diffusivity tensor is substantially lower than that for suspensions of rigid particles, and is a function of particle deformability. At low area fractions, the diffusivity depends linearly on the area fraction; this is due to the finite displacement of two deformable drops passing each other under the influence of a simple shear flow. As a result, the diffusivity of dilute suspensions of liquid drops is higher than that of rigid spheres.

Interfacial mobility and particle deformability work synergistically to make the suspension adapt more easily to the shearing environment of the imposed flow. The present simulations address the particular case where the viscosity of the drops is equal to that of the ambient fluid. As the viscosity of the drop fluid is raised, the drops tend to behave like rigid particles, and we expect that the motion of the suspension will undergo significant changes. Liquid capsules, such as cells enclosed by elastic membranes, may be highly deformable even in the absence of interfacial mobility. The motion of suspensions of such particles may thus be expected to be intermediate between that of liquid drops and solid particles, and will be discussed in a forthcoming article.

We thank Dr A. Kraynik and Dr Hua Zhou for useful comments and discussions. This research was supported by the National Science Foundation, the Department of Energy, the American Chemical Society, and SUN Microsystems Corporation. Computing time was provided by the San Diego Supercomputer Center.

REFERENCES

ABRAMOWITZ, M. & STEGUN, I. A. 1972 *Handbook of Mathematical Functions.* Dover.

ACRIVOS, A., BATCHELOR, G. K., HINCH, E. J., KOCH, D. L. & MAURI, R. 1992 Longitudinal shear-induced diffusion of spheres in a dilute suspension. *J. Fluid Mech.* **240**, 651–657.

BARNES, H. A., EDWARDS, M. F. & WOODCOCK, L. V. 1987 Applications of computer simulations to dense suspension rheology. *Chem. Engng Sci.* **42**, 591–608.

BATCHELOR, G. K. 1974 Transport properties of two-phase materials with random structure. *Ann. Rev. Fluid Mech.* **6**, 227–255.

BOSSIS, G. & BRADY, J. F. 1984 Dynamic simulation of sheared suspension. I. General method. *J. Chem. Phys.* **80**, 5141–5154.

BOSSIS, G. & BRADY, J. F. 1987 Self-diffusion of Brownian particles in concentrated suspensions under shear. *J. Chem. Phys.* **87**, 5437–5448.

BOSSIS, G. & BRADY, J. F. 1989 The rheology of Brownian suspensions. *J. Chem. Phys.* **91**, 1866–1874.

BRADY, J. F. & BOSSIS, G. 1985 The rheology of concentrated suspensions of spheres in simple shear flow by numerical simulation. *J. Fluid Mech.* **155**, 105–129.

BRADY, J. F. & BOSSIS, G. 1988 Stokesian Dynamics. *Ann. Rev. Fluid Mech.* **20**, 111–157.

CHADRASEKHAR, S. 1943 Stochastic problems in physics and astronomy. *Rev. Mod. Phys.* **15**, 1–89.

CHANG, C. & POWELL, R. L. 1993 Dynamic simulation of bimodal suspensions of hydrodynamically interacting spherical particles. *J. Fluid Mech.* **253**, 1–25.

CHANG, C. & POWELL, R. L. 1994*a* The rheology of bimodal hard-sphere dispersions. *Phys. Fluids* **6**, 1628–1636.

CHANG, C. & POWELL, R. L. 1994*b* Self-diffusion of bimodal suspensions of hydrodynamically interacting spherical particles in shearing flow. *J. Fluid Mech.* **281**, 51–80.

CHARLES, R. 1996 Dynamic simulation of the flow of suspension of liquid drops. PhD dissertation, University of California, San Diego.

CLAEYS, I. L. & BRADY, J. F. 1993 Suspensions of prolate spheroids in Stokes flow. Part 1. *J. Fluid Mech.* **251**, 411–442.

DAVIS, R. H., SCHONBERG, J. A. & RALLISON, J. M. 1989 The lubrication force between two viscous drops. *Phys. Fluids* A **1**, 77–81.

ECKSTEIN, E. C., BAILEY, D. G. & SHAPIRO, A. H. 1977 Self-diffusion of particles in shear flow of a suspension. *J. Fluid Mech.* **79**, 191–208.

FRANKEL, N. A. & ACRIVOS, A. 1967 On the viscosity of a concentrated suspension of solid spheres. *Chem. Engng Sci.* **22**, 847–853.

KAUSCH, H. H., FESKO, D. G. & TSCHOEGL, N. W. 1971 The random packing of circles in a plane. *J. Colloid Interface Sci.* **37**, 603–611.

KENNEDY, M. R., POZRIKIDIS, C. & SKALAK, R. 1994 Motion and deformation of liquid drops and the rheology of dilute emulsions in simple shear flow. *Computers Fluids* **23**, 251–278.

KIM, S. & KARRILA, S. 1991 *Microhydrodynamics*. Butterworth.

LADD, A. J. 1990 Hydrodynamic transport coefficients of random dispersions of hard spheres. *J. Chem. Phys.* **93**, 3484–3494.

LEIGHTON, D. & ACRIVOS, A. 1987 Measurement of shear-induced self-diffusion in concentrated suspensions of spheres. *J. Fluid Mech.* **177**, 109–131.

LI, X., ZHOU, H. & POZRIKIDIS, C. 1995 A numerical study of the shearing motion of emulsions and foams. *J. Fluid Mech.* **286**, 379–404.

MONIN, A. S. & YAGLOM, A. M. 1965 *Statistical Fluid Mechanics: Mechanics of Turbulence*, Vol. I. MIT Press.

POZRIKIDIS, C. 1992 *Boundary Integral and Singularity Methods for Linearized Viscous Flow*. Cambridge University Press.

POZRIKIDIS, C. 1993 On the transient motion of ordered suspensions of liquid drops. *J. Fluid Mech.* **246**, 301–320.

POZRIKIDIS, C. 1995 Stokes flow in the presence of interfaces. In *Boundary Element Applications in Fluid Mechanics*. Computational Mechanics Publications, Southampton, UK.

POZRIKIDIS, C. 1996*a* Computation of periodic Green's functions of Stokes flow. *J. Engng Maths* (in press).

POZRIKIDIS, C. 1996*b* Heat or mass transport from a suspended particle at low Péclet numbers. *J. Fluid Mech.* (submitted).

REINELT, D. A. & KRAYNIK, A. M. 1990 On the shearing flow of foams and concentrated emulsions. *J. Fluid Mech.* **215**, 431–455.

ROCO, M. C. 1993 *Fundamentals of Thermal and Statistical Physics*. McGraw Hill.

STONE, H. 1994 Dynamics of drop deformation and breakup in viscous fluids. *Ann. Rev. Fluid Mech.* **26**, 65–102.

WANG, H., ZINCHENKO, A. Z. & DAVIS, R. H. 1994 The collision rate of small drops in linear flow fields. *J. Fluid Mech.* **265**, 161–188.

YIANTSIOS, S. G. & DAVIS, R. H. 1991 Close approach and deformation of two viscous drops due to gravity and van der Waals forces. *J. Colloid Interface Sci.* **144**, 412–433.

ZHANG, X. & DAVIS, R. H. 1991 The collisions of small drops due to Brownian and gravitational motion. *J. Fluid Mech.* **230**, 479–504.

ZHOU, H. & POZRIKIDIS, C. 1993*a* The flow of suspensions in channels: single files of drops. *Phys. Fluids* A **5**, 311–324.

ZHOU, H. & POZRIKIDIS, C. 1993*b* The flow of ordered and random suspensions of two-dimensional drops in a channel. *J. Fluid Mech.* **255**, 103–127.

ZHOU, H. & POZRIKIDIS, C. 1994 Pressure-driven flow of suspensions of liquid drops. *Phys. Fluids* A **6**, 80–94.

ZHOU, H. & POZRIKIDIS, C. 1995 Deformation of capsules with incompressible interfaces in simple shear flow. *J. Fluid Mech.* **283**, 175–200.